Tactile quality control with biomimetic active touch

Nathan F. Lepora, *Member, IEEE*, Benjamin Ward-Cherrier, *Student Member, IEEE*

***Abstract*—Fully autonomous factories of the future will need automated quality control processes to monitor products during manufacture. Here we demonstrate that an artificial tactile system offers a solution to autonomous quality inspection, using a biomimetic tactile fingertip mounted as end-effector on an industrial arm. The study considers a task of gap width inspection suitable for judging parts alignment, although the methods apply generally. An active perception method implements optimal decision making while controlling sensor location, which was recently shown to attain superresolved spatial perception. In consequence, gap width is estimated to sub-millimeter accuracy comparable to human discrimination performance and is robust to uncertainty in test object placement. We conclude that an artificial tactile system of the type here offers an ideal solution to automated quality control on the production line.**

***Index Terms*—Force and Tactile Sensing; Biomimetics**

I. INTRODUCTION

A potentially important application area for artificial tactile fingertips is to explore and inspect surfaces of interest, for example as part of a manufacturing production process. An influential modern view in production is that the process used to manufacture a product is a key determiner of quality [1], a view proposed to counterbalance the traditional perspective that quality is determined mainly by design. From a view of enabling greater quality in production, we consider here a tactile surface inspection robot comprising a biomimetic fingertip mounted as an end-effector on a robot arm (Fig. 1).

Autonomous surface inspection is well-studied in the field of non-destructive testing with non-contact methods such as microwaves [2] and ultrasound [3]. An important example application is gap and step quality control between assembled panels in automotive manufacturing, where state-of-the-art devices include laser scanners and image mapping systems. Optical devices, by virtue of not contacting the surface, are necessarily indirect. However, there can be complexities when adjacent surfaces differ in reflectivity or are transparent, and so the human sense of touch is still commonly used on the production line (Fig. 2).

This letter demonstrates that artificial tactile systems offer an accurate and reliable solution to automated quality control. Because artificial touch sensing relies on direct surface contact, issues complicating optical and other indirect methods are avoided. The advantages of human touch for quality control that underlie its use on the production line can be leveraged, while limitations arising from human operators (cost, fatigue, subjectivity) can be addressed with an artificial system.

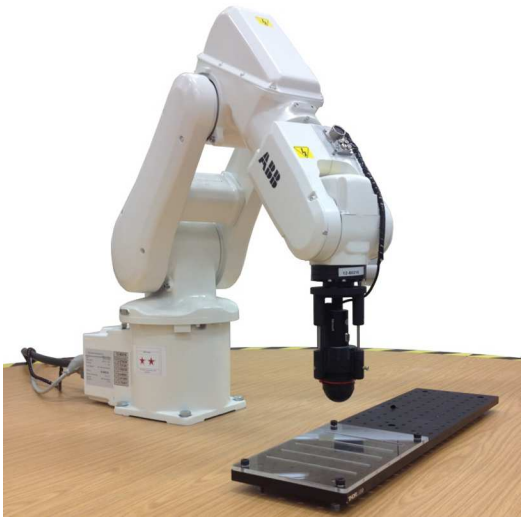

Fig. 1: Tactile quality control robot, comprising a tactile fingertip (the TacTip) mounted as end effector on a robot arm.

Fig. 2: Tactile quality control on a production line.

This study considers a specific task of gap width inspection, although the methods apply more generally. The task here is to identify a gap of unknown width (range 0.25-5 mm) with unknown contact depth (range 0-5.5 mm) below the tactile sensor (Fig. 4), using repeated taps of a biomimetic tactile fingertip. An active perception method is used to implement optimal decision making while controlling sensor location [4], [5], which was recently shown to attain superresolved spatial perception [6], [7]. In consequence, gap width is estimated to 0.35 mm, which is comparable to human discrimination performance. Thus, an artificial tactile system of the type here offers an accurate and reliable solution to automated quality control on the production line.

Manuscript received: August 28, 2015; revised December 10, 2015; accepted January 7, 2016. This letter was recommended for publication by Editor J. Wen upon evaluation of the Associate Editor and reviewers' comments. N. Lepora was supported by the Engineering and Physical Sciences Research Council (EPSRC) under grant EP/M02993X/1 and B. Ward-Cherrier was supported by an EPSRC DTP studentship. Data from this paper is available at http://lepora.com/publications.htm and http://doi.org/bxzj

The authors are with the Bristol Robotics Laboratory (BRL) and the Department of Engineering Mathematics, University of Bristol, U.K. (email: n.lepora@bristol.ac.uk, bw14452@bristol.ac.uk)

Digital Object Identifier (DOI): see top of this page.

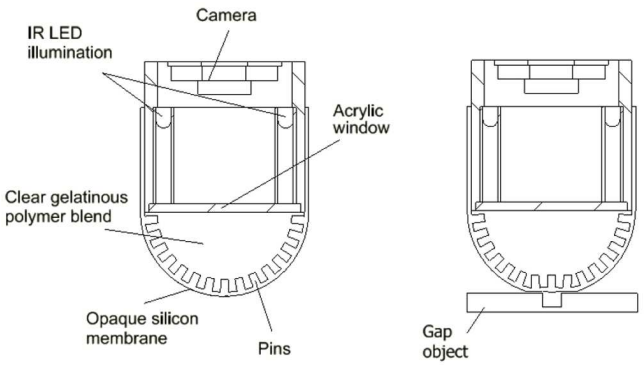

Fig. 3: Diagram of the TacTip (left) with pins shown on the inside surface of a silicon membrane, which are LED illuminated and imaged by an internal camera. The right diagram is a representation of the deformation of the membrane as the finger pad impinges on a test object (a gap stimulus).

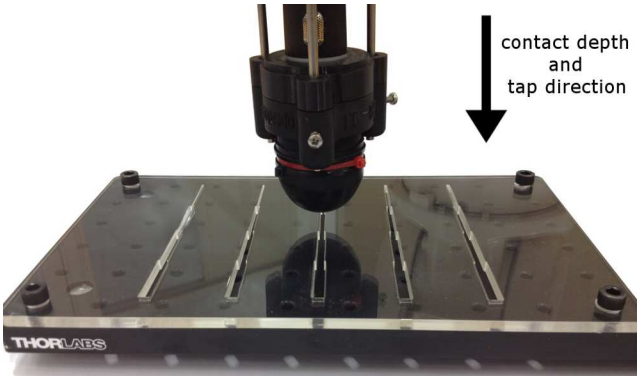

Fig. 4: Stimulus for assessing gap width. 20 gaps of widths 0.25 mm to 5 mm (in 0.25 mm equal steps) are laser cut in a perspex sheet. Each gap has length 30 mm, sufficient to span the 40 mm TacTip width.

II. BACKGROUND AND RELATED WORK

Our approach for artificial touch sensing uses a statistical framework in which training data is first sampled from exemplar stimuli and then used to identify unknown stimuli. The statistical approach is combined with active perception to control how the sensor contacts the stimulus during sensing, and used with biomimetic tactile fingertips.

Statistical approaches can be viewed as contrasting with 'model-based' approaches for identifying tactile stimuli. Model-based approaches use an inverse physical model of the sensor response to infer the stimulus [8], [9]; hence, they generalize over many stimuli, but physical models can be complicated and difficult to fit or invert. In contrast, statistical approaches sample the environment directly and use Bayes' rule for the inversion; hence, the models are relatively easy to obtain, but are specialist to the type of stimuli trained over. For example, training with gap stimuli would not generalize well to testing over curvature.

Active perception [10] is a key part of attaining good accuracy in the gap detection task considered here, referring to a combination of interpreting the sensory data with control based on the interpreted tactile data [11], [12]. The benefit of active perception is that the control of the tactile sensor can aid the interpretation of the sensory data, for example by making a more informative contact with a stimulus. Recent work on active touch with biomimetic fingertips has focussed on algorithms for sensor control and perception. An artificial finger that dynamically feels texture [13] used a neural network controller for curiosity-driven exploration to learn motor skills for active perception [14]. Another study used closed loop control of exploratory movements with a biomimetic fingertip to discriminate compliance [15].

A benefit of statistical approaches is that they combine readily with active perception. One example, termed Bayesian exploration, selects tactile data (modulating speed and contact force) that disambiguates a leading percept from its alternatives [16]. Another approach, termed active Bayesian perception, sets a control policy to guide sensor location ('where') during optimal decision making of object identity ('what') [4], [5], typically fixating the sensor over the object. This latter method is robust to position uncertainty [5] and can result in superresolved spatial perception surpassing the sensor resolution [6], [7], motivating its use here.

Active touch has been demonstrated on several biomimetic fingertips having discrete tactile elements (taxels), including capacitive sensors (*e.g.* iCub fingertip) [4]–[6], MEMS sensors [13] and barometric sensors (*e.g.* biotac) [15], [16]. Here we use an optical tactile sensor called the TacTip (Tactile fingerTip) developed at Bristol Robotics Laboratory [7], [17]–[19]. The TacTip's principal novelty as an optical tactile sensor is that it has an array of pins molded inside the skin that indicate deformations of the surface, with displacements analogous to sensor readings from taxel-based devices.

III. METHODS

A. Details of the tactile sensor and data collection

1) The Tactile fingertip: The TacTip is an optical tactile sensor that has several highly useful properties (Fig. 3): (i) the casing is 3D-printed and hence readily customizable and inexpensive; (ii) it uses a standard CCD web-camera (LifeCam Cinema HD, Microsoft) to collect data, which is also inexpensive and connects to a PC via a USB interface; (iii) it has a molded silicon outer membrane that is robust to wear and easily replaced if damaged; and (iv) between the outer membrane and the electronics is a clear compliant gel (RTV27906, Techsil UK) that enables tactile sensing through compression and protects the delicate parts of the sensor.

The design of the TacTip used here has a 40 mm diameter hemispherical sensor pad with 532 pins arrayed on its underside (of which 40 are selected for analysis). Six LEDs mounted on a ring around the base of the pad illuminate the pins, whose tips have been coated with white paint to contrast with the black silicon outer membrane.

2) Data collection: The TacTip is mounted as an end-effector on a six degree-of-freedom robot arm (IRB 120, ABB Robotics) that can precisely and repeatedly position the sensor (absolute repeatability 0.01 mm).

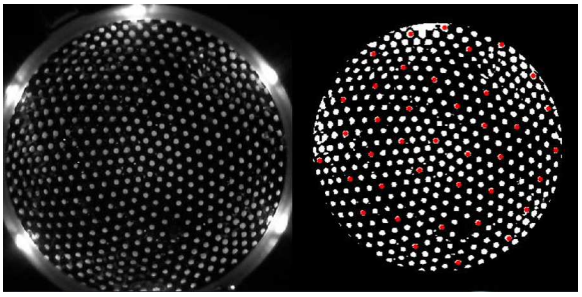

Fig. 5: Left: typical image captured by the internal camera. Right: filtered image with just 40 pins tracked (shown in red).

The test stimuli are 20 gaps of width 0.25 mm to 5 mm in 0.25 mm steps (Fig. 4). These were laser cut into a flat perspex sheet at 30 mm intervals. The TacTip was mounted with its (hemispherical) sensing surface oriented downwards in the direction of tapping motion normal to the sheet. Data were collected while the tactile sensor tapped 6 mm down onto the test gap followed by a move back up, then a 0.05 mm downwards displacement before the next tap. Altogether 110 taps were made per gap over 5.5 mm (110 taps), with a 2 sec time series of pressure readings ($N_{\text{samples}} = 40$) taken for each tap. All data used in this letter were collected twice to give distinct training and test sets, ensuring that all results are based on sampling from an independent data set to that used to train the classifier.

3) Data preprocessing: The TacTip collects tactile data as images (resolution 640×480 pixels, sampled at ∼20 fps), which are filtered to detect and track displacements of pins molded to the underside of the outer membrane. Images were captured and preprocessed using opencv (http://opencv.org/). For pin detection, a Gaussian spatial filter with adaptive threshold was applied to each image; the adaptive threshold allowed for varying luminosity across the image field (Fig. 5). For pin tracking, the Lucas-Kanade algorithm was applied to $N_{\text{samples}} = 40$ consecutive images for each tap, to give the optical flow of pins during the contact. Individual pin displacements were then inferred by integrating the flow field from the initial pin locations.

A subset of the 532 detected pins were used as tactile elements (Fig. 5), reducing computational requirements and removing data redundancy. 40 selected pins were chosen with at least 4 mm separation (shown colored in Figs. 7). The two-dimensional s_x and s_y displacements of these pins $s_k(j)$ are treated as distinct data dimensions, with $1 \leq k \leq N_{\text{dim}} = 80$ and $1 \leq j \leq N_{\text{samples}} = 40$.

B. Active and passive biomimetic tactile perception

We use a Bayesian approach for biomimetic tactile perception based on sequential analysis methods for optimal decision making [20]. Sequential analysis is a statistical technique for hypothesis selection over sequentially sampled data until reaching a stopping condition [21], which commonly takes the form of a threshold on the posterior belief.

Active biomimetic perception [4]–[7] accumulates belief for the perceptual classes by successively contacting the stimulus

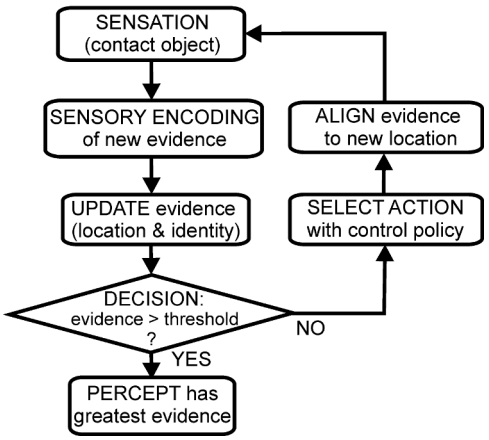

Fig. 6: Biomimetic active perception implements a sensation-action loop that accumulates evidence for multiple distinct perceptual hypotheses while a control policy selects appropriate actions to relocate the sensor based on that evidence.

until a posterior belief reaches threshold while utilizing a posterior-dependent control policy to move the sensor (Fig. 3). In previous work on tactile superresolution, only perception over location was considered [6], [7]; here, we consider perception over both stimulus location x_l (depth) and identity w_i (gap width), represented by class pairs (x_l, w_i).

Formally, the perception algorithms apply to sequences of contact data $z_{1:t} = \{z_1, \cdots, z_t\}$, with each contact encoded as an N_{dim}-dimensional time series of sensor values,

$$z_t = \{s_k(j) \ : \ 1 \leq j \leq N_{\text{samples}}, \ 1 \leq k \leq N_{\text{dim}}\}, \qquad (1)$$

with indices j, k labeling the sample and data dimension, and N_{samples} is the number of time samples in a contact.

The following analysis gives a Bayesian estimation of location x_l, $1 \leq l \leq N_{\text{loc}}$ and identity w_i, $1 \leq l \leq N_{\text{id}}$ of an object, considered one of a set of distinct punctual locations and stimulus identities (here $N_{\text{loc}} = 11$ locations spanning 5.5 mm and $N_{\text{loc}} = 20$ gap identities are used).

1) Measurement model and likelihood estimation: The likelihoods $P(z_t|x_l, w_i)$ of contact data z_t being from a location and identity class (x_l, w_i) assume a measurement model that averages the individual log-probabilities for each sample over the training data,

$$\log P(z_t|x_l, w_i) = \sum_{k=1}^{N_{\text{dim}}} \sum_{j=1}^{N_{\text{samples}}} \frac{\log P_k(s_k(j)|x_l, w_i)}{N_{\text{samples}} N_{\text{dim}}}. \qquad (2)$$

Following other work on robot tactile perception [20], [22], [23], the sample distributions $P_k(s_k|x_l, w_i)$ are found with a histogram method. Binning the sensor values s_k (for dimension k) into equal intervals I_b, $1 \leq b \leq N_{\text{bins}}$ over their range (here $N_{\text{bins}} = 100$), the histogram counts $n_{kli}(b)$ are over all training data in that location and identity class,

$$P_k(s_k|x_l, w_i) = P_k(b|x_l, w_i) = \frac{n_{kli}(b) + \epsilon}{\sum_{b=1}^{N_{\text{bins}}} n_{kli}(b)}, \qquad (3)$$

appropriately normalized so that $\sum_{b=1}^{N_{\text{bins}}} P_k(b|x_l, w_i) = 1$. A small regularization constant $\epsilon \ll 1$ ensures that all log likelihoods (2) are well-defined if any histogram bin is empty.

2) Bayesian belief update: Bayes' rule is used after each successive test contact z_t to recursively update the posterior beliefs $P(x_l, w_i|z_{1:t})$ for the perceptual classes with the likelihoods $P(z_t|x_l, w_i)$ of that contact data

$$P(x_l, w_i|z_{1:t}) = \frac{P(z_t|x_l, w_i)P(x_l, w_i|z_{1:t-1})}{P(z_t|z_{1:t-1})}, \quad (4)$$

from background information given by the prior location beliefs $P(x_l, w_i|z_{1:t-1})$ (*i.e.* the posterior beliefs from the preceding contact). The marginal probabilities are given by

$$P(z_t|z_{1:t-1}) = \sum_{i,l=1}^{N_{\rm id},N_{\rm loc}} P(z_t|x_l, w_i)P(x_l, w_i|z_{1:t-1}). \quad (5)$$

A sequence of contacts $z_1, \cdots, z_t$ results in a sequence of posterior beliefs $P(x_l, w_i|z_1), \cdots, P(x_l, w_i|z_{1:t})$ initialized from uniform priors $P(x_l, w_i|z_0) = 1/N_{\rm loc}N_{\rm id}$.

3) Final decision: Here the task is to determine identity (gap width), and so the stopping condition uses the marginal identity beliefs summed over all location classes,

$$P(w_i|z_{1:t}) = \sum_{l=1}^{N_{\rm loc}} P(x_l, w_i|z_{1:t}). \quad (6)$$

Then the Bayesian update (4,5) stops with decision $w_{\rm dec}$ when the identity belief passes a decision threshold $\theta_{\rm dec}$:

$$\text{if any } P(w_i|z_{1:t}) > \theta_{\rm dec} \text{ then } w_{\rm dec} = \arg\max_{w_i} P(w_i|z_{1:t}). \quad (7)$$

This belief threshold $\theta_{\rm dec}$ is a free parameter that adjusts the balance between decision time $t_{\rm dec}$ and decision accuracy.

4) Active perception: Active perception uses a posterior-dependent control policy π to move the sensor $x \leftarrow x + \pi$ during the perceptual process. For simplicity, we consider this to depend only on an intermediate estimate of location

$$x_{\rm est}(t) = \arg\max_{x_l} P(x_l|z_{1:t}), \quad (8)$$

from location beliefs summed over all identity classes

$$P(x_l|z_{1:t}) = \sum_{i=1}^{N_{\rm id}} P(x_l, w_i|z_{1:t}). \quad (9)$$

Three control policies are considered, one active and the other two passive:

1. *Active 'fixation point' control* [4]–[6] attempts to move the sensor to a predefined fixation point $x_{\rm fix}$ relative to the object assuming it is at $x_{\rm est}$ on the object,

$$x \leftarrow x + \pi\left(x_{\rm est}\right), \;\; \pi(x_{\rm est}) = x_{\rm fix} - x_{\rm est}. \quad (10)$$

Provided the fixation point is set to be a good location for perception, the perception will progressively improve during the decision making process from an initially unknown location where perception may be poor.

2. *Passive stationary perception* never moves the sensor from the initial location class where it contacts the object: $\pi = 0$.

3. *Passive random perception* moves the sensor randomly, with uniform distribution $\Delta x \sim U(1, x_{N_{\rm loc}})$, $p(x) = 1/N_{\rm loc}$ (and locations x defined modulo $N_{\rm loc}$ to keep within range).

Algorithm Active Bayesian perception

```
% Training
for i=1 to N_id do
  for l=1 to N_loc do
    Sample contact data z = {s_k(j)} from class (x_l,w_i)
    Pre-compute P(s_k|x_l, w_i) using histogram method
  end for
end for
% Testing
Initialize flat priors P(x_l, w_i|z_0) = 1/N_loc N_id at t = 0
while max_i Σ_l P(x_l, w_i|z_1:t) < θ_dec do
  Update contact number t ← t + 1
  Sample contact data z_t = {s_k(j)}
  Compute likelihoods P(z_t|x_l, w_i) using P(s_k|x_l, w_i)
  Bayesian belief update of P(x_l, w_i|z_1:t)
  Active control policy: x ← x + π(P(x_l, w_i|z_1:t))
  Re-align beliefs P(x_l, w_i|z_1:t) ← P(x_{l−Δl}, w_i|z_1:t)
end while
Decision w_dec = arg max_{w_i} Σ_l P(x_l, w_i|z_1:t)
```

After a move of Δl location classes, the beliefs $P(x_l, w_i|z_{1:t})$ are kept aligned with the sensor by shifting the class probabilities by the number of classes moved

$$P(x_l, w_i|z_{1:t}) \leftarrow P(x_{l-\Delta l}, w_i|z_{1:t}) \text{ if } 1 \le x_{l-\Delta l} \le N_{\rm loc},$$
$$\text{else } P(x_l, w_i|z_{1:t}) \leftarrow P(x_1, w_i|z_{1:t}) \text{ or } P(x_{N_{\rm loc}}, w_i|z_{1:t}).$$

For simplicity, the (undetermined) probability shifted from outside the location range is assumed uniform and given by the existing probability at that extremity of the range (probabilities are then renormalized to have unit sum).

5) Virtual environment validation: The aim of the data collection is to make a 'virtual environment' in which gap identification accuracy can be evaluated off-line. The identity error is quantified with the mean absolute error

$$e_{\rm id}(x, w) = \langle |w - w_{\rm dec}| \rangle, \quad (11)$$

with the ensemble average $\langle\cdot\rangle$ evaluated over all test runs with the same true class (x, w). An overall measure of performance averages these errors over all (x, w) classes

$$\bar{e}_{\rm id} = \sum_{i,l=1}^{N_{\rm id},N_{\rm loc}} \frac{e_{\rm id}(x_l, w_i)}{N_{\rm id}N_{\rm loc}}. \quad (12)$$

The decision time $t_{\rm dec}(x, w)$ and mean decision time $\bar{t}_{\rm dec}$ are defined similarly.

A Monte Carlo validation ensures good statistics by averaging errors over test data drawn randomly from all locations. Typically, we averaged 5000 distinct Monte Carlo runs for each value of the decision threshold $\theta_{\rm dec}$, randomly sampling over all location and identity classes.

IV. RESULTS

A. Inspection of data

Contact data (Fig. 7) were collected while the TacTip tactile fingertip tapped repeatedly against each of the test objects, comprising 20 gaps of widths 0.25 mm to 5 mm in

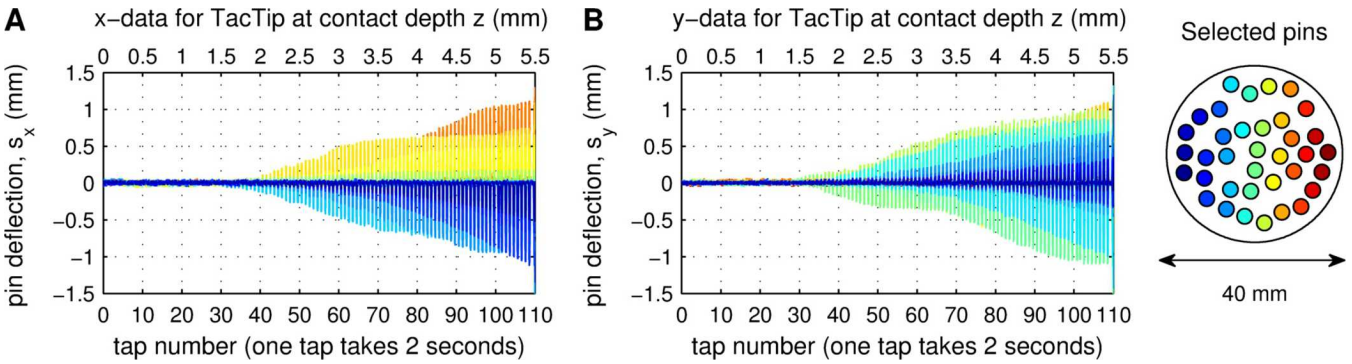

Fig. 7: Tactile data for TacTip contacting a single gap (0.25 mm width) over a 5.5 mm location range with 110 taps. The plots show the pin s_x-displacements (panel A) and s_y-displacements (panel B). Taxels are colored according to their location on the contact pad (color scheme in right panel).

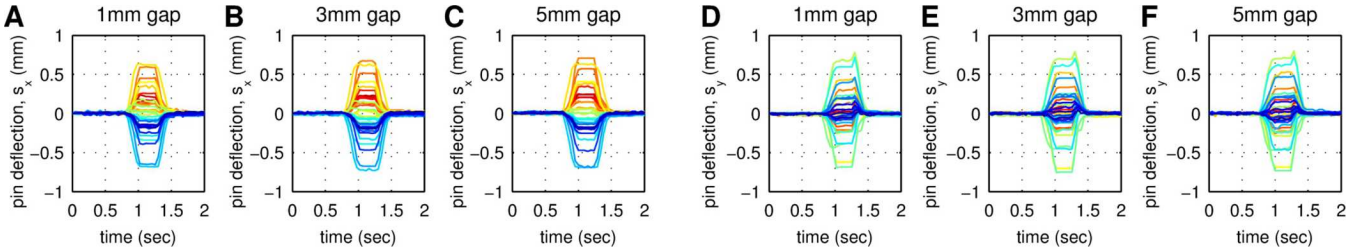

Fig. 8: Tactile data for TacTip contacting 3 of the 20 gaps (widths 1 mm, 3 mm and 5 mm) at a vertical location of 4 mm (80th tap). Taxel readings s are shown for the pin s_x-displacements (panels A,B,C) and s_y-displacements (panels D,E,F). Taxels are colored by location on the contact pad (see Fig. 7).

0.25 mm steps. A 5.5 mm range of vertical displacements were considered for the start (and end) position of each tap, using 110 taps separated by 0.05 mm depth (giving a total of 2200 discrete taps over all gaps). Pin displacements from individual taps (visible in Fig. 8) typically take about 250 ms to reach response peak amplitude, followed by a plateau for 250 ms then a return to baseline also taking 250 ms. Contact features from the stimulus are encoded in the time-series response of each pin deflection, including its temporal dynamics and peak value reached.

The vertical contact position of the TacTip relative to the gap has a noticeable effect on both the peak s_x and s_y taxel readings (Figs 7A,B). Taps with the greatest depth in the location range are the strongest, decreasing smoothly towards those of least depth, with an upper region of about 1.5 mm (30 taps) where the TacTip does not contact the surface.

At first sight, the gap width does not noticably affect the two-dimensional time series of s_x and s_y taxel displacements (Fig. 8) for 3 gaps (1 mm, 3 mm, 5 mm) spaced across the 20 test gaps. However, closer inspection reveals subtle changes in the relative pin displacements that could indicate differences in gap width. The effect of these differences in pin deflection is analyzed in the following results.

B. Active and passive perception of gap width

The accuracy of the TacTip for gap inspection is assessed with both active and passive robot perception (closed- and open-loop control policies). We use a Bayesian perception method that updates the posterior beliefs for $N_{\rm id} = 20$ identity (gap width) classes and $N_{\rm loc} = 11$ location (depth) classes until a belief on an identity class reaches decision threshold. This belief threshold determines both the decision time $t_{\rm dec}$, or number of contacts to make a decision, and also the identification accuracy $e_{\rm id}$. Results are generated with a Monte Carlo procedure using the data as a virtual environment (Sec. III-B5).

For both active and passive perception, the mean errors for gap width $\bar{e}_{\rm id}$ (averaged over initial location and identity) decrease with increasing mean decision times $\bar{t}_{\rm dec}$ to reach close to minimum asymptote after ∼8-12 contacts (Fig. 9). This tradeoff between mean decision duration and accuracy follows from standard decision theory, since accuracy improves as more evidence is used to form a decision.

Comparison of best accuracies for estimating gap width shows that active perception with a fixation control policy is best, with mean error $e_{\rm id} \sim 0.35$ mm (1.3 identity classes) over 8-12 taps (with fixation depth $x_{\rm fix} = 4.75$ mm). Passive perception with a random policy is next best, with mean error $e_{\rm id} \sim 0.6$ mm (2.2 identity classes) over 8-12 taps. Passive perception with a stationary control policy is worst, with mean error $e_{\rm id} \sim 0.8$ mm (3.2 identity classes) over 8-12 taps.

These decision errors are with no information about the initial contact depth of the sensor relative to the test object. Active perception uses intermediate information about depth during decision formation to guide the sensor to a good location, enabling accurate inspection of the gap width.

Therefore provided the sensor can be actively controlled to contact the test gap at optimal contact depth, then the mean

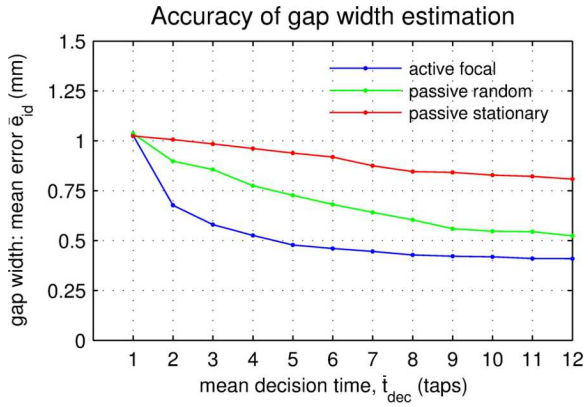

Fig. 9: Gap width accuracy for active (blue) and passive random (green) or stationary (red curve) perception. Mean errors $\bar{e}_{\mathrm{id}}$ are plotted against mean decision time $\bar{t}_{\mathrm{dec}}$. Results are averaged over all stimuli and initial contact locations, with 5000 Monte Carlo iterations per data point.

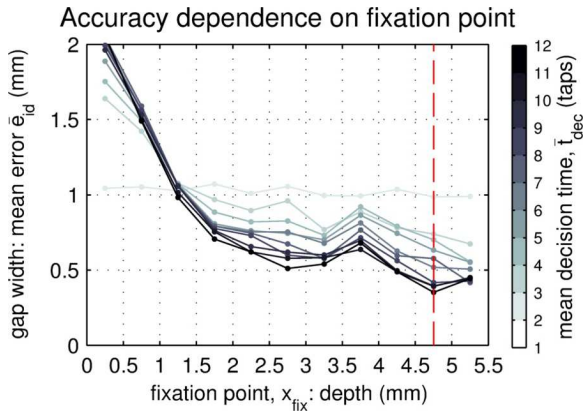

Fig. 10: Dependence of mean error $\bar{e}_{\mathrm{id}}$ on fixation point of the active control policy over a range of decision times (grey shading). The optimal perceptual accuracy (after 12 taps) is at the fixation point shown by the red dashed line ($\mathrm{x}_{\mathrm{fix}} = 4.75\,\mathrm{mm}$), which is the fixation point used in Fig. 9.

identity (gap width) error can approach $\bar{e}_{\mathrm{id}} \sim 0.35\,\mathrm{mm}$ over the 0.25-5 mm range of widths.

C. Optimal fixation depth for active perception

Active perception with a fixation point control policy is the most accurate method for assessing gap width, compared to passive methods for perception. However, the control policy is specified by a free parameter, the fixation depth, which was assumed to be at an optimal depth for the perception. This dependence of perception on fixation depth is now examined, to justify this assumption and determine the optimal contact depth. Results are again generated with a Monte Carlo procedure similarly to Sec. IV-C, now with the fixation point varied across the range of depth locations.

Probing active perception over contact depth, the gap width mean errors $\bar{e}_{\mathrm{id}}$ vary strongly with fixation point x_{fix} over the depth location range (Fig. 10; gray shading denotes mean decision time $\bar{t}_{\mathrm{dec}}$ corresponding to the x-axis on Fig. 9).

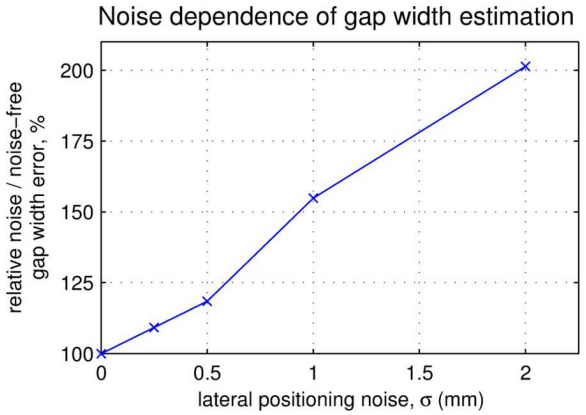

Fig. 11: Dependence of gap width estimation error $\bar{e}_{\mathrm{id}}$ on uncertainty placing the sensor laterally relative to the gap. The performance degradation is represented by the ratio of the estimation error to that of the noise-free case $\bar{e}_{\mathrm{id}}(\sigma)/\bar{e}_{\mathrm{id}}(0)$, for lateral uncertainty distributed over $[-\sigma, \sigma]$ mm.

The best fixation depths are at the deepest contacts (rightmost range), and the poorest at depths where the fingertip contacts weakly or not at all (leftmost range). The optimal location for fixation is shown (red dashed line at 4.75 mm), corresponding to the location class with lowest mean error after 12 taps, which was used to generate the results in Fig. 9 (Sec. IV-B).

D. Dependence on positioning uncertainty

Finally, we examine how the above results depend on the accuracy of sensor placement over the gap. Thus far we have considered positioning uncertainty only in depth, which is controlled through active perception to give the lowest mean error $\bar{e}_{\mathrm{id}} \sim 0.35\,\mathrm{mm}$ after 8-12 contacts (Fig. 9). However, in a realistic scenario there may also be uncertainty placing the sensor laterally across the gap.

The experiments and analysis from Secs IV-B, IV-C are repeated with noise in the test data from randomly varying the lateral placement of the sensor relative to the gap (here sampled from a uniform distribution $[-\sigma, \sigma]$). Four magnitudes of noise are considered: $\sigma = 0.25, 0.5, 1.0, 2.0\,\mathrm{mm}$. An identical analysis to Sec. IV-B can then be carried out on these datasets, which is summarized by the mean errors $\bar{e}_{\mathrm{id}}(\sigma)$ over 8-12 contacts. These errors are displayed relative to the noise-free case $\bar{e}_{\mathrm{id}}(\sigma)/\bar{e}_{\mathrm{id}}(0)$ (Fig. 11).

Noise in the lateral placement of the sensor degrades the performance of gap width estimation $\bar{e}_{\mathrm{id}}$. The performance decreases with increasing noise (Fig. 11), with estimation errors doubling for $\sigma = 2\,\mathrm{mm}$. For noise magnitude $\sigma \leq 0.5\,\mathrm{mm}$, gap width estimation is within 25% of the noise-free case.

Our purpose here is to verify that the methods are robust to (moderate) amounts of noise in positioning the sensor in a direction not controlled by active perception. Similar results should apply also to noise in pose (roll, pitch and yaw). In general, we expect a smooth degradation of estimation performance with increasing location uncertainty. If the degradation becomes too large, then active perception could be applied in the direction causing the uncertainty to reduce this source of error in the estimation performance.

V. Discussion

In this study, we demonstrated that narrow gaps (0.25 mm to 5 mm) could be inspected to high ($\bar{e}_{\rm id} \sim 0.35$ mm) accuracy with a biomimetic tactile fingertip (the TacTip) mounted as an end-effector on a robot arm. This accuracy was attained under uncertainty about the location of the gap relative to the sensor, by using active touch to control sensor position during decision making of gap width. This accuracy is superresolved compared to the 4 mm sensor resolution given by the spacing between pins on the sensor [7].

Our attained accuracy rivals that of human touch. With static ($\sim$1 sec) touches against embossed spatial patterns, subjects estimated relative interval size to 0.3 mm and Vernier alignment to 0.4 mm [24]. (Vernier acuity refers to separation of two parallel lines, analogous to gap width.) Biomimetic superresolution is thus analogous to human tactile hyperacuity, which is typically an order of magnitude better than the two-point discrimination interval ($\sim$3 mm) and the density of (type SA-I) mechanoreceptors in the human fingertip ($\sim$70/cm^2).

Can this inspection accuracy be improved? Finer acuity could arise from modifying the sensor hardware and perception method, to go beyond human performance. A miniaturized TacTip [18] would better detect smaller features, compared with the 40 mm diameter device considered here. Also, other exploratory procedures could be superior to taps, related to how humans tailor tactile exploration to the task at hand [25]. With these improvements, we expect an identification accuracy $\lesssim$100 μm is readily attainable, and possibly far finer.

For an effective quality control system in practice, the active perception of gap width would need to be combined with guidance systems to probe the entire product/vehicle. One method to achieve this exploration would be to use 3D vision systems to identify locations of interest (*e.g.* joins between panels); the tactile sensor could then be moved to each of these locations, after which the closed loop tactile control takes over to fine tune the sensor location for optimal perception. A complementary method for exploration would be to use the tactile sensor to autonomously track edges or other surface features, as can be achieved with related methods for tactile contour following [26].

Therefore we conclude that an artificial tactile system of the type proposed here can offer an accurate and reliable solution to automated quality control on the production line. For the best accuracies, closed-loop active feedback is necessary to control the contact depth of the tactile sensor against the surface. The entire system can be implemented with an inexpensive 3D-printed tactile sensor mounted as end-effector on an industrial robot arm.

VI. Conclusion

This study demonstrates tactile quality control at an accuracy comparable to human performance with an inexpensive, biomimetic fingertip (the TacTip) mounted as an end-effector on an industrial robot arm. The performance relies on using active perception to control the location of the sensor relative to the test object. We conclude that an artificial tactile system of the type proposed here can offer an accurate and reliable solution to automated quality control on the production line.

References

[1] R. Inman, D. Blumenfeld, N. Huang, and J. Li. Designing production systems for quality: research opportunities from an automotive industry perspective. *International journal of production research*, 41(9):1953–1971, 2003.

[2] R. Zoughi. *Microwave Non-Destructive Testing and Evaluation Principles*, volume 4. Springer Science & Business Media, 2000.

[3] J. Blitz and G. Simpson. *Ultrasonic methods of non-destructive testing*, volume 2. Springer Science & Business Media, 1996.

[4] N. Lepora, U. Martinez-Hernandez, and T. Prescott. Active bayesian perception for simultaneous object localization and identification. In *Robotics: Science and Systems*, 2013.

[5] N. Lepora, U. Martinez-Hernandez, and T. Prescott. Active touch for robust perception under position uncertainty. In *Proc. IEEE Int. Conf. Robot. Autom. (ICRA)*, pages 3005–3010, 2013.

[6] N. Lepora, U. Martinez-Hernandez, M. Evans, L. Natale, G. Metta, and T.J. Prescott. Tactile superresolution and biomimetic hyperacuity. *IEEE Transactions on Robotics*, 31(3):605–618, 2015.

[7] N. Lepora and B. Ward-Cherrier. Superresolution with an optical tactile sensor. In *Proc. IEEE/RSJ Int. Conf. Intell. Robots Syst. (IROS)*, pages 2686–2691, 2015.

[8] L. Muscari, L. Seminara, F. Mastrogiovanni, M. Valle, M. Capurro, and G. Cannata. Real-time reconstruction of contact shapes for large area robot skin. In *Proc. IEEE Int. Conf. Robot. Autom. (ICRA)*, pages 2360–2366, 2013.

[9] L. Seminara, M. Capurro, and M. Valle. Tactile data processing method for the reconstruction of contact force distributions. *Mechatronics*, 27:28–37, 2015.

[10] R. Bajcsy. Active perception. *Proceedings of the IEEE*, 76(8):966–1005, 1988.

[11] T. Prescott, M. Diamond, and A. Wing. Active touch sensing. *Philosophical Transactions of the Royal Society B: Biological Sciences*, 366(1581):2989–2995, 2011.

[12] N. Lepora. Active tactile perception. In *Scholarpedia of Touch*, pages 151–159. Atlantis Press, 2016.

[13] C. Oddo, M. Controzzi, L. Beccai, C. Cipriani, and M. Carrozza. Roughness encoding for discrimination of surfaces in artificial active-touch. *IEEE Transactions on Robotics*, 27(3):522–533, 2011.

[14] L. Pape, C. Oddo, M. Controzzi, C. Cipriani, A. Förster, M. Carrozza, and J. Schmidhuber. Learning tactile skills through curious exploration. *Frontiers in neurorobotics*, 6:6, 2012.

[15] Z. Su, J. Fishel, T. Yamamoto, and G. Loeb. Use of tactile feedback to control exploratory movements to characterize object compliance. *Frontiers in neurorobotics*, 6:7, 2012.

[16] J. Fishel and G. Loeb. Bayesian exploration for intelligent identification of textures. *Frontiers in Neurorobotics*, 6:4, 2012.

[17] C. Chorley, C. Melhuish, T. Pipe, and J. Rossiter. Development of a tactile sensor based on biologically inspired edge encoding. In *International Conference Advanced Robotics (ICAR)*, pages 1–6, 2009.

[18] B. Winstone, G. Griffiths, C. Melhuish, T. Pipe, and J. Rossiter. Tactiptactile fingertip device, challenges in reduction of size to ready for robot hand integration. In *Int. Conf. Robotics and Biomimetics (ROBIO)*, pages 160–166, 2012.

[19] T. Assaf, C. Roke, J. Rossiter, T. Pipe, and C. Melhuish. Seeing by touch: Evaluation of a soft biologically-inspired artificial fingertip in real-time active touch. *Sensors*, 14(2):2561–2577, 2014.

[20] N. Lepora, C.W. Fox, M. Evans, M. Diamond, K. Gurney, and T. Prescott. Optimal decision-making in mammals: insights from a robot study of rodent texture discrimination. *Journal of The Royal Society Interface*, 9(72):1517–1528, 2012.

[21] A. Wald. *Sequential analysis*. John Wiley and Sons (NY), 1947.

[22] N. Lepora, M. Evans, C. Fox, M. Diamond, K. Gurney, and T. Prescott. Naive bayes texture classification applied to whisker data from a moving robot. *Int. Joint Conf. Neural Networks (IJCNN)*, pages 1–8, 2010.

[23] N. Lepora, J. Sullivan, B. Mitchinson, M. Pearson, K. Gurney, and T. Prescott. Brain-inspired bayesian perception for biomimetic robot touch. In *Proc. IEEE Int. Conf. Robot. Autom. (ICRA)*, pages 5111 –5116, 2012.

[24] J. Loomis. An investigation of tactile hyperacuity. *Sensory Processes*, 3:289–302, 1979.

[25] S. Lederman and R. Klatzky. Hand movements: A window into haptic object recognition. *Cognitive psychology*, 19(3):342–368, 1987.

[26] U. Martinez-Hernandez, T. Dodd, L. Natale, G. Metta, T. Prescott, and N. Lepora. Active contour following to explore object shape with robot touch. In *World Haptics Conference (WHC)*, pages 341–346, 2013.